Carpathian Journal of Earth and Environmental Sciences August 2023, Vol. 18, No. 2, p. 307 – 322; DOI:10.26471/cjees/2023/018/261

TOWARDS UAV ASSISTED MONITORING OF AQUATIC VEGETATION WITHIN LARGE RIVERS – THE MIDDLE DANUBE (SERBIA)

Maja NOVKOVIĆ[1*], Dušanka CVIJANOVIĆ[1], Minučer MESAROŠ[1], Dragoslav PAVIĆ[1], Nusret DREŠKOVIĆ[2], Đurađ MILOŠEVIĆ[3], Ana ANĐELKOVIĆ[4], Bojan DAMNJANOVIĆ[5], & Snežana RADULOVIĆ[1,2]

*[1]University of Novi Sad, Faculty of Sciences, Trg Dositeja Obradovića 3, 21000 Novi Sad, Serbia e-mail: maja.novkovic@dbe.uns.ac.rs (*corresponding author); dusanka.cvijanovic@dbe.uns.ac.rs minucer.mesaros@dgt.uns.ac.rs, dragoslav.pavic@dgt.uns.ac.rs, snezana.radulovic@dbe.uns.ac.rs*

[2]University of Sarajevo, Faculty of Science, Department of Geography, Zmaja od Bosne 33-35, 71000, Sarajevo, Bosnia and Herzegovina e-mail: nusretd@pmf.unsa.ba

[3]University of Niš, Faculty of Sciences and Mathematics, Department of Biology and Ecology, Višegradska 33, 18000 Niš, Serbia e-mail: djuradj@pmf.ni.ac.rs

[4]Institute for Plant Protection and Environment, Department of Weed Research, Teodora Drajzera 9, 11040 Belgrade, Serbia e-mail: ana.andjelkovic21@gmail.com

[5]Academy of Applied Studies Šabac, Unit for Medical, Technological and Business Studies, Hajduk Veljkova 10, 15000 Šabac, Serbia; bdamnjanovic@live.com

Abstract: UAV technologies provide a time- and cost-efficient framework for a variety of environmental monitoring domains. It also increases data resolution and provides new insights into observed objects and phenomena, especially within the difficult-to-access and complex for monitoring aquatic habitats. The objective of this study was to develop UAV-based acquisition and GIS-based image processing guidelines for aquatic macrophyte detection and monitoring in large temperate rivers. According to the European standard CEN EN -14184:2014, the assessment of aquatic macrophytes should be performed using the transect approach. Large rivers, such as the Danube, represent an exception and should be evaluated using 1km transects. Therefore, seven transects of the Middle Danube in Serbia were simultaneously surveyed using traditional field methods and novel UAV technology. UAV images were acquired using RGB and multispectral cameras carried by a fixed-wing drone. The images were processed and orthomosaics were classified using Object Based Image Analysis (OBIA), to create digital GIS maps of the river transects. During the traditional monitoring approach, the relative abundance of 22 macrophyte species was recorded along the transects. Using the UAV technology and OBIA approach eight macrophyte classes were distinguished based on dominant macrophyte taxa or plant life form traits. Aquatic macrophytes were 'almost perfectly' distinguished from the orthomosaics, achieving a high classification accuracy of 96 % / 88 % / 0.84 for RGB and 94 % / 97 % / 0.95 Producers /Users accuracy/Kappa index for the multispectral approach. Individual macrophyte classes accuracy varied between 0.5 and 1 Kappa and were generally higher for the multispectral imagery approach. Although the resolution of the taxonomic data is lower, UAV monitoring provided the necessary spatial context of macrophytes distribution and absolute area occupied by macrophytes. It also provided information on the diversity and distribution of habitats along the river. Therefore, the UAV-assisted monitoring approach described in this study can be effectively integrated into macrophyte monitoring during large river expeditions such as the JDS.

Keywords: UAV, GIS, Remote sensing, Aquatic macrophytes, Environmental monitoring, The Danube River

1. INTRODUCTION

Monitoring of the diversity, structure, and ecological characteristics of biota in rivers and lakes represents the basis for fundamental and applied research of freshwater ecosystems. When it comes to the assessment of aquatic vegetation within European rivers, the transect approach represents the ‘gold standard’, although there are differences concerning transect length, scoring system, monitoring

frequency, and data evaluation and interpretation methods (Birk et al., 2010).

Monitoring schemes for large rivers usually do not follow the standards for any given area or river type but represent exceptional strategies developed to make the monitoring process feasible and yet as reliable as possible. Monitoring strategies for aquatic vegetation are usually evaluating minimal acceptable area and are using robust assessment methods including evaluations from boats and ships or using aerial photographs, which produce low-resolution data (Birk et al., 2012), and are spatially and temporally limited, and time and money consuming especially considering monitoring of large areas (Sojka et al., 2019). Ecological monitoring of the Danube River relies on the Joint Danube Survey (JDS) expeditions, realized once every six years. The strategy for aquatic vegetation assessment follows the European Standard EN 14184: 2003 i.e., EN 14184: 2014, although the standard itself make an exception for the Danube River. The result of the macrophytes monitoring campaign is the ecological status of the selected river sections, which usually comprise only a small fraction of the total river course.

Development of the Unmanned Aerial Vehicles (UAV) technology has enabled highly flexible and efficient data collection with high spatial, temporal, and spectral resolution, which offer a variety of possibilities for environmental monitoring (Pande-Chhetri et al., 2017; Manfreda et al., 2018). The development of the GIS provided new tools for environmental monitoring and mapping (Jaskuła & Sojka, 2019) among which the image analysing tools gave encouraging results for aquatic vegetation assessment.

Various researchers have reported successful evaluation of aquatic and riparian vegetation in general (Ventura et al., 2018; Brinkhoff et al., 2018; Taddia et al., 2020), detection of specific ecological groups (Visser et al., 2018; Visser et al., 2013; Husson, 2016; Husson et al., 2017; Villoslada et al., 2020), and individual native or invasive species (Flynn & Chapra, 2014; Pande-Chhetri et al., 2017; Bolch et al., 2021; Chabot et al., 2016; Chabot et al., 2018, Brooks et al., 2019). Copter-type (multirotor) drones are prevalent, mostly because of their availability, manoeuvrability, and price. Nevertheless, in the domain of large-scale research (more than 1km^2) fixed-wing drones appear to be a more suitable option (Tmušić et al., 2020). During the first several years most of the studies used RGB cameras (Flynn & Chapra, 2014; Husson et al., 2014; Husson, 2016; Husson et al., 2017; Pande-Chhetri et al., 2017; Marcaccio et al., 2015; Visser et al., 2015; Visser et al., 2018; Ventura et al., 2018; Michez et al., 2016; Stocks et al., 2019), but with the development of the specialized UAV multispectral (MSP) cameras in the recent years there is significant amount of studies testing the possibilities they offer (Chabot et al., 2016; Chabot et al., 2018; De Luca et al., 2019; Brinkhoff et al., 2018; Taddia et al., 2020; Brooks et al., 2019; Song & Park, 2020; Villoslada et al., 2020; Agioutanti, 2022). There are also two dominant image analysing approaches - pixel-based and object-based (OBIA) image classification. Pixel-based approach classifies images pixel by pixel, based on their spectral characteristics (Pande-Chhetri et al., 2017). However, with the improvement of UAV images resolution, the OBIA approach emerged as a more suitable solution (Pande-Chhetri et al., 2017; Sibaruddin et al., 2018) and is used in the plethora of studies (Husson, 2016; Husson et al., 2017; Chabot et al., 2016; Chabot et al., 2018; Sibaruddin et al., 2018; Visser et al., 2013; Visser et al., 2018; Ventura et al., 2018; Díaz-Varela et al., 2018; Brooks et al., 2019). OBIA approach includes the image segmentation, and subsequent classification of the created segments. It also tends to include additional contextual information, shape, texture, and spectral characteristics, of the image objects into classification process (Sibaruddin et al., 2018). Machine learning algorithms have been recognized as the most successful image classification approach, among which the *Random Forest* classifier stands out (Husson, 2016; Husson et al., 2017; Villoslada et al., 2020; van Iersel et al., 2018). Considering that there are currently no standards instructing researchers and stakeholders on how to obtain, analyse, and interpret data, all existing studies could be considered pioneering research within a new multidisciplinary field uniformly and comparably. This field could improve and optimize the methodology for assessing aquatic vegetation in the future.

This study represents the first attempt to integrate available UAV assessment tools into the existing traditional monitoring scheme and enable collection of higher resolution aquatic vegetation data within the Middle Danube area in Serbia.

The aim of this study was to develop UAV-based acquisition and GIS-based image processing guidelines for detection and monitoring of aquatic vegetation in large temperate rivers. In order to achieve the main goals of this study, the following tasks were set: 1) to collect aquatic vegetation data along the Middle Danube sections using traditional survey methods; 2) to create, perform, and optimize a UAV protocol for collecting vegetation data at the same river sections; 3) to carry out the object based image classification of UAV aquatic vegetation data; 4) to compare results of the standard vegetation monitoring

and UAV based approach with recommendations for the following JDS and other large river expeditions.

Integration of remote sensing within traditional monitoring could provide new insights about aquatic habitats (Jaskuła & Sojka, 2019). By standardizing, UAV tools would enable the processing of larger areas in shorter time frames and ease method calibration, intercalibration, and harmonization process. In this way, the temporal dynamics of aquatic vegetation, hydromophological characteristics, but also increasing anthropogenic pressures and impacts along the watercourse could be efficiently monitored.

2. STUDY AREA

Fieldwork was conducted at four locations along the lower section of the Danube River in Serbia (Figure 1). The goal was to include the sections of the river with different floristic and hydro-morphological characteristics, which would allow testing of the approach on diverse habitats and vegetation types.

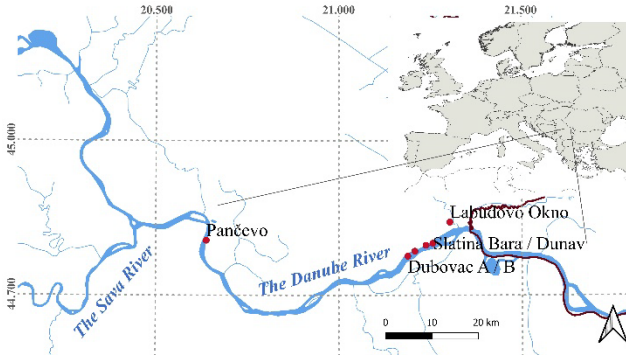

Figure 1. Selected sections of the Danube River in the Middle Danube area in Serbia

1. Pančevo – Two typical subsequent 1 km river stretches. Silt substrate and sand riverbank with the slight slope, up to 1 m height. Mixed poplar-willow riparian forest with poplar tree plantation in the background. Pančevo_A - Upstream quarter of the section is used as a weekend lodging area with a sporadically resectioned, embanked, and steep bank. Pančevo_B - Dominantly pristine.

2. Dubovac – Two subsequent embanked 1 km river stretches. Silt and sand-gravel mixture substrate with steep, up to 3 m high concrete blocks embankment, with a cultivated poached pasture in the background. Dubovac_A – Extremely shallow former flooded forest area, with remaining sporadic tree roots and boulders. Part of the vegetated sandbar. Dubovac_B - Deeper embanked river section, only partly encompasses the sand sidebar.

3. Slatina – two individual non-subsequent sections. Slatina_Bara - The Danube River oxbow connected with the river main course. Part of Dubovački rit flooding area. Silt substrate with a gently sloped earth/silt bank, with tall emergent vegetation. Slatina_Dunav - Sand-gravel shallow river sidebar at the bottom of a high loess section. Slightly sloped low riverbank with an almost vertical loess section above. Sporadic willow trees and tall herbs.

4. Labudovo okno – oxbow of the Danube River directly connected to the river's main course. Silt substrate and an almost flat sand bank, with sporadic willow trees and tall herbs.

3. MATERIALS AND METHODS

3.1. Aquatic vegetation survey

Aquatic vegetation of the selected sections was assessed twofold, using transect and plot survey approaches. Transect vegetation survey was performed according to the Joint Danube Survey (JDS) methodology, which was developed in accordance with the *Guidance for the surveying of aquatic macrophytes in running waters* (CEN – EN 14184, 2014). Aquatic vegetation was assessed through 1 km transects evaluated from a small boat slowly floating along the banks, with at least two stops (200 and 700 m) for detailed plant inventory and sampling (JDS4, 2021). The presence, abundance, and life form of each macrophyte species present in the water were recorded. Macrophyte abundance was assessed using the Kohler five-point scale for aquatic vegetation of running waters (Kohler, 1978; Kohler & Janauer, 1995). Life forms of the plants were determined according to the MIDCC (Multifunctional Integrated Study, Danube Corridor and Catchment). Each time when a floristic and/or structural change in the vegetation was observed along the transect, additional stops were made. At each stop, macrophytes were assessed using vegetation plot survey approach. Present species were quantified using the five-point Kohler scale (Kohler, 1978). Depending on the size of the stand, the plot's size ranged from 0.5 to 3 m in radius. In the case of large uniform stands several subsequent plots were recorded to improve interpretation of the photogrammetry products. Evaluated transects and plots were georeferenced using a GPS device and the time spent was noted.

3.2. Flight

River sections were recorded with the fixed-wing *Sensefly eBee X* drone using RGB *S.O.D.A.* and multispectral *Parrot Sequoia* cameras. Sensefly S.O.D.A camera with a 1” 20 Mpx RGB sensor is the

first camera specifically designed for professional drone photogrammetry. Parrot Sequoia multispectral camera captures imagery across four narrow spectral bands with 1.2 Mpx monochrome sensors centered in the Green – 550 nm, Red – 660 nm and Near Infrared – 790 nm regions with 40 nm bandwidth and Red Edge – 735 nm wavelength with 10 nm bandwidth, it also captures RGB photos with 16 Mpx sensor.

Aerial images were acquired through two subsequent flights at each location. The flight altitudes were 185-215 m above the ground, with 80% longitudinal and 60% lateral image overlap. Orthomosaic resolution of 0.02 m/pix was targeted as it enables the distinction of singular individuals of most aquatic macrophytes from the photos. All flights were performed within one day (04.09.2020., 9-19 h) at optimal meteorological conditions.

3.3. UAV workflow

3.3.1. S.O.D.A – RGB imagery

UAV-based geotagged images were block adjusted and stitched into individual georeferenced orthomosaics using default settings of the *Adjust* tool within the ArcGIS Pro 2.6.0 software.

Orthomosaic segmentation was performed using *LargeScaleMeanShift* algorithm of Orfeo Toolbox (OTB) 7.2.0 within the QGIS 3.16.3-Hannover software. Segmentation process groups the neighboring pixels into discrete entities based on their spectral characteristics and spatial distribution, forming a new polygon layer. Different range and spatial radius values were tested to determine optimal segmentation parameters (De Luca et al., 2019). Range factor was changed by 1 degree, while spatial radius was changed by 10 degrees. Products were visually evaluated after each iteration (Pande-Chhetri et al., 2017; De Luca et al., 2019). Minimum segment size of 50 pixels was set to prevent creation of small objects which could cause scattered classification (Ventura et al., 2018). This enabled isolation of smallest distinguishable image objects given the image resolution as suggested in Sibaruddin et al., (2018), which were individual *Trapa sp.* plants or *Nymphea/Nuphar* leaves. Similar approach was used by De Luca et al., (2019) and De Marinis et al., (2021). If the segment size was lower than the set threshold it was merged with the most similar surrounding segment.

Before further analysis *Area of Interest* (AOI) polygons were created for each transect. Bank, riparian areas, terrestrial vegetation, and artificial constructions beyond the scope of the research were clipped out (Chabot et al., 2018; Jiménez-Jiménez et al., 2020; Villoslada et al., 2020). In this way, the UAV approach was coordinated with the JDS macrophyte assessment methodology, focusing only on aquatic vegetation within the river channel.

After segmentation, a set of RGB and texture indices were calculated for each orthomosaic (Tables 1 and 2). RGB indices were calculated using *Raster calculator* tool (Barbosa et al., 2019), while the Texture indices were compiled using *FeatureExtraction* tools of OTB, and r.texture tool of the GrassGIS providers in QGIS. Texture indices were compiled based on the first axis of PCA (*Principal components analysis*) analysis of RGB the orthomosaics (Kupidura, 2019). The mean value of all indexes was calculated for each segment using *Zonal statistics* tool in QGIS. Calculated values were used as objects classification attributes in order to increase the classification accuracy (Pande-Chhetri et al., 2017). Training and validation data sets were created by expert based visual interpretation, which was feasible due to extremely high resolution of orthomosaics (Ventura et al., 2018; Chabot et al., 2018). Training datasets were created by manual selection of 50 evenly distributed representative reference objects for each feature class. Macrophyte data collected through traditional field methods were used as ground truth and reference data during this process, but were not solely sufficient and fully adequate for successful and automatic extraction of the training dataset (Chabot et al., 2018).

Validation datasets were automatically extracted from the segmentation layer based on the 400 points created with *Random points* tool in QGIS (Pande-Chhetri et al., 2017; Ventura et al., 2018). The goal was the differentiation of macrophytes to the species level, but due to extremely small dimensions, morphological and spectral similarity of some species, that was not always possible. Therefore, the trait-based approach was combined with the species-based during the feature classes determination. On the other hand, due to different spectral and texture characteristics of phenological and ecological variability of species some classes needed to be divided into several feature subclasses (Pande-Chhetri et al., 2017). Feature classes were named after the most dominant plant taxon (Husson et al., 2016) or ecological trait.

Supervised object classification (OBIA) was performed in QGIS with Orfeo Toolbox (OTB) 7.2.0 provider using *Random Forest* classifier. According to several studies OBIA was recognized as superior comparing with the pixel-based classification methods (Pande-Chhetri et al., 2017; van Iersel et al., 2018) or manual mapping (Husson et al., 2016) when it comes to high resolution remote sensing data (Ventura et al., 2018). *Random forest* classifier was chosen as it

Table 1. Spectral indices which were used as classification attributes.

Abbreviation	Index	Formula	S.O.D.A.	Sequoia	Reference
MGRVI	*Modified Green Red Vegetation Index*	$(G)^2-(R)^2/(G)^2+(R)^2$	*	*	Bendig et al., 2015.
RGBVI	*Red Green Blue Vegetation Index*	$(G)^2-(B*R)/(G)^2+(B*R)$	*		Bendig et al., 2015.
GRVI MPRI	*Green Red Vegetation Index* *Modified Photochemical reflectance Index*	G−R/ G+R	*	*	Tucker CJ, 1979. Yang et al., 2008.
NDRGI	*Normalized difference red green index*	(R –G)/ (R + G)	*	*	Yang et al., 2008.
GLI	*Green Leaf Index*	2G - R – B/ 2G + R + B	*		Louhaichi et al., 2001.
ExG	*Excess of green*	2G – R – B	*		Woebbecke et al., 1995.
G-B	*Green-Blue difference*	G-B	*		
G-R	*Green-Red difference*	G-R	*		
R-B	*Red-Blue difference*	R-B	*		
NDVI	*Normalized Difference Vegetation Index*	NIR – R/ NIR + R		*	Rouse et al., 1974
NDWI	*Normalized Difference Water Index*	G – NIR/ G + NIR		*	McFeeters, 1996
GreenNDVI	*Green Normalized Difference Vegetation Index*	NIR – G/ NIR + G		*	Gitelson et al., 1996.
ModifiedNDVI	*Modified Normalized Difference Vegetation Index*	RedEdge – R/ RedEdge + R		*	Brooks et al., 2019.
NDREI	*Normalized NIR – RedEdge Vegetation Index*	NIR – RedEdge/ NIR + RedEdge		*	Gitelson et al., 1994.
NGRDI	*Normalized Red – Green Difference Index*	G – R/ G + R		*	Pearson et al., 1972.

Table 2. Texture indices which were used as classification attributes.

Abbreviation	**Index**	**Feature**	**S.O.D.A.**	**Sequoia**	**Reference**
r.tex	*r.texture*	*Sum Average (SA)*	*	*	
		Inverse Difference Moment (IDM)	*	*	
		Angular Second Moment (ASM)		*	
		Sum Entropy (SE)		*	
SFS	*Structural Feature Set*	*SFS'Length*		*	Huang et al., 2007
		SFS'Width		*	
		SFS'PSI	*	*	
		SFS'W-Mean		*	
		SFS'Ratio		*	
		SFS'SD	*	*	
HAR or GLCM	*Haralic Texture* or *Gray Level Co-Occurrence Matrix*	*Energy*		*	Kupidura, 2019.
		Entropy	*	*	
		Correlation		*	
		Inverse Difference Moment	*	*	
		Innertia	*	*	
		Cluster Shade		*	
		Cluster Prominence		*	
		Haralick Correlation		*	

represents one of the most successful, redundancy, and noise resilient classification algorithms for the remote sensing data (Chabot et al., 2018; Villoslada et al., 2020). It is efficient in distinguishing spectrally similar image feature classes (Husson et al., 2017), can operate with nonlinear variables (Villoslada et al., 2020), and is

most suitable to OBIA classification approach (Ma et al., 2017). *TrainVectorClassifier* tool of QGIS allows the classification optimization through the modification of algorithm parameters values. Different combinations of Maximum depth of trees (5/10/15/20), Maximum number of trees in forest (100/150/200/225/250) (Chabot et al., 2018) and Minimum number of samples in each node (7/10) were tested during the classifier optimization phase. Classification accuracy and adequacy was assessed using automatically calculated per polygon Kappa index and visual interpretation, similar as in Taddia et al., (2020) which used overall accuracy and visual inspection.

Classifications were visually evaluated, and poorly classified areas were determined. Training data sets were improved by adding new reference polygons for each inadequately allocated feature class. The training process was repeated, and orthomosaics were reclassified. This processing step was included to provide the targeted increase of classification accuracy. After the reclassification corresponding feature classes were merged in order to create digital maps which provide ecologically meaningful representation of aquatic macrophytes and plant life forms distribution along the river sections. Each macrophyte class is represented with a unique color, and relative percentage of the AOI is calculated, as well as the absolute area covered by each class expressed in m^2.

Twofold accuracy analyses, per-polygon and per-pixel approaches (Ye et al., 2018) were applied for classification and reclassification phase of aquatic vegetation map production, verifying accuracy of the classification algorithm (Husson et al., 2017). Accuracy of final maps was assessed using 'per-pixel' approach (Husson et al., 2017). 'Per polygon' approach focuses on a number of correctly classified segments, while 'per pixel' approach assess the correctly classified area (number of pixels) of each feature class (Ye et al., 2018; Stehman & Wickham, 2011). *TrainVectorClassifier* tool calculated per-polygon general performance Kappa index (KI) and overall accuracy (OA). Per-pixel accuracy analyses were performed using *Accuracy* tool of *Semi-Automatic Plugin in QGIS* calculating Kapa hat index (KHI) and overall accuracy (OA) for each map, but also User's (UA), Producer's accuracy (PA), and Kappa Hat index for each feature class (Ventura et al., 2018; Kaplan et al., 2022). Kappa index were interpreted according to Landis & Koch, 1977. Visser et al., (2018) pointed out debate about appropriateness of Kappa index as classification accuracy measure, but as it is still commonly applied in available research it was used in this study as well.

3.3.2. Parrot Sequoia – Multispetral imagery

Multispectral imagery workflow followed the one developed for the RGB S.O.D.A imagery. Nevertheless, some alterations needed to be implemented. UAV images collected via Parrot Sequoia camera were preprocessed and geotagged via *Postflight* module of eMotion 3.5.0 software using drone and eMotion flight logs. Geotagged images were further processed using default settings of *Processing* module of the Pix4D mapper 4.2.27. Multispectral images were radiometrically calibrated using Sequoia Reflectance Panel and R, G, NIR and RedEdge reflectance maps were rendered (Chabot et al., 2018; Brinkhoff et al., 2018; Taddia et al., 2020; Agioutanti, 2022).

Before the segmentation NDVI and NDWI indices were calculated for every survey site. NDVI index was suggested as the addition to the R, G and NIR bands by (Chabot et al., 2018) for better demarcation of the above-the water features during the segmentation process. NDWI index was additionally calculated to enhance the open water areas (McFeeters, 1996) because the segmentation of multiband raster compiled of R, G, B and NDVI layers lacked to distinguish submerged vegetation from the open water area. As reported in (McFeeters, 1996) NDVI and NDWI have opposite enhancement focuses on terrestrial vegetation and open water subsequently. Pixel values of the input reflectance maps and indices were normalized by multiplying with 255 as suggested in (McFeeters, 1996; De Luca et al., 2019; Agioutanti, 2022). Normalized layers were merged into one multiband raster layer (Chabot et al., 2018; De Luca et al., 2019; Taddia et al., 2020). AOI polygons were created, multiband rasters were clipped, and segmentation process was performed. During the segmentation process range radius values of 5, 7 and 10 were tested, while spatial radius was changed in increments of 5 degrees. Due to coarser multispectral orthomosaics' resolution, minimum segment size was changed to 20 pixels. In that way similar segmentation results could be obtained. Selection of the additional spectral indices was based on the bands availability and reported potential applicability by various authors (Villa et al., 2014; Brooks et al., 2019; Song & Park, 2020;Villoslada et al., 2020) (Table 1). PCA analyses were carried out on multiband rasters (R, G, NIR, NDVI, NDWI) and the first axes were used to calculate the texture indices (Table 2). Training and validation datasets form the S.O.D.A. workflow was spatially adjusted in accordance with the MSP orthomosaics, and image feature classes were revised before the classification process.

Effort, time and data resolution obtained implementing the traditional monitoring scheme and UAV based tools were compared. Best aspects of each

approach were selected, and the novel combined monitoring protocol is proposed.

4. RESULTS

4.1. Aquatic vegetation survey

Aquatic vegetation was assessed along seven transects of the lower course of the Danube River in Serbia. Due to the terrain configuration, it was not always possible to inspect the full 1 km transect length. Four river transects were investigated from the boat, while the remaining three were assessed from the shore. A total of 22 aquatic macrophyte species were recorded in 5 plant life forms (Table 3). The average time needed to assess the transect was around 40 min, ranging 25-100 min, depending on macrophyte abundance, diversity of the vegetation structure, and river section hydromophological characteristics. Depending on vegetation complexity and spatial distribution, 19-46 additional vegetation plots were recorded and geotagged along the transects.

4.2. Flight

UAV imagery was collected through eight flights at four survey locations (Pančevo, Dubovac, Slatina and Labudovo okno). At three locations eBee+ drone was able to cover two transects per one flight. Average time spent to capture 1 km long and about 300 m wide transect at a height of 185 m for MSP and 215 m for RGB flights was about 15 min. In order to achieve the optimal lateral and longitudinal image overlap the drone was collecting about 200-250 photos with the S.O.D.A RGB camera, and around 600-1200 photos with Sequoia MSP camera, covering about 30 ha area per each river section.

4.3. UAV workflow

During the image adjustment process, some of the photos were removed from the collections due to inadequate image properties. Adjusted images were stitched into the orthomosaics with an average ground resolution of 0.024 m/pix for RGB and 0.078 m/pix for MSP imagery. Orthomosaics completely covered the intended study areas, while only orthomosaic for Pančevo survey site resulted with unsatisfactory area coverage. Instead of covering the two transects of 1 km length, the software generated one in length of 300 m for the RGB data and none for the MSP data.

During the segmentation process spatial radius of 30 and range radius of 10 have been chosen as the most suitable combination for the RGB orthomosaics. In the case of MSP orthomosaics, the range radius was lowered to 7, as the value of 10 could not distinguish submerged vegetation from the surrounding water. AOI polygons were 1 km long, while the width varied between 10 m at Pančevo study site and 300 m at Dubovac. Prior to the classification, 20 spectral and texture characteristics were calculated to describe each segment of the RGB and 32 to describe segments within the MSP approach (Table 1, 2).

Emergent and floating species could be mostly determined to the species level, except for the yellow and white waterlily whose leaves could not be fully differentiated. Single individuals of small-scale species such as *Salvinia natans*, *Lemna* sp., *Spirodela* sp. Could not be distinguished from the orthomosaics, not even *Hydrocharis morsus ranae* and *Nymphoides peltate*, unless they were abundantly present at the spot. Information about submerged species under the floating

Table 3. Abundance of macrophyte species recorded using the standard monitoring approach.

	Salvinia natans (L.) All.	*Ceratophyllum demersum* L.	*Spirodela polyrhiza* (L.)	*Lemna minor* L.	*Trapa natans* L.	*Myriophyllum spicatum* L.	*Lemna trisulca* L.	*Filamentous algae*	*Najas marina* L.	*Azolla filiculoides* Lam.	*Hydrocharis morsus-ranae* L.	*Nuphar lutea* (L.) Sm.	*Nymphaea alba* L.	*Potamogeton nodosus* Poir.	*Potamogeton perfoliatus* L.	*Vallisneria spiralis* L.	*Potamogeton gramineus* L.	*Microalgae at the bottom*	*Phragmites australis (Cav.)*	*Lemna gibba* L.	*Schoenoplectus lacustris* (L.) Palla	*Nymphoides peltata* (S. G.	*Butomus umbellatus* L.	*Stuckenia pectinata* (L.)
Slatina_Bara		5						3					4					4	5			4		
Slatina_Dunav	4	5	4	3	5	3	1	3	3		2			3	3	3	3	5	3				4	
Dubovac_A	4	5	3	3				3	4	3				3										
Dubovac_B	4	5										2	3	3	1		1							
Labudovo okno	5	5	2	2	5	2	2	2	3	2					4	4			4	2	3	3		
Pančevo_A		4						2						2					2				2	4
Pančevo_B		5	2					3								1							2	5

vegetation layer could not be assessed as it could not be seen from the air. All submerged species were classified as 'submerged vegetation' feature class, as it was not possible to determine the exact species. On the other hand, *Trapa natans*, waterlilies and *Phragmites communis* needed to be represented with more than one feature class due to spectral differences plants manifested along the transects. In total, 20 feature classes were determined: twelve aquatic vegetation feature classes, plus two classes of algae occurrence, one terrestrial vegetation group and a miscellaneous group of five non-vegetation image feature classes.

During the classifier optimization phase 40 different combinations of *Random Forest* parameters were tested. Kappa index of the analyses ranged from moderate to almost perfect for both, RGB: 0.52 - 0.86 and MSP approach: 0.53 - 0.81. In both approaches - RGB and MSP *Minimum number of samples in each node* 7 produced better results. In the case of RGB imagery *Maximum depth of trees* of 10 produced the best results, while for the MSP the results were less conclusive. Changing the *Maximum number of trees in forest* caused minimal difference in the classification results, in over 90 % of cases it caused less than 0.03 units of change of Kappa index. Examining the matrix of tested combinations none of the options could be declared the absolute best, hence the additional visual inspection of classifications was conducted. Finally, the following combination of parameters was chosen as the best option: *Minimum number of samples in each node*: 7; *Maximum depth of trees*: 10; *Maximum number of trees in forest*: 225. Adding the reclassification phase to the workflow led to the general increase of the classification accuracy, observing both 'per polygon' and 'per pixel' accuracy (Table 4). Even in the situations where improvements in classification accuracy metrics were not substantial, a more realistic map of the river transect was created. 'Per pixel' accuracy tests generally resulted with higher classification accuracy than 'per polygon' tests.

Image feature classes were merged in 16 ecologically meaningful categories and digital maps of each investigated transect were produced. This step also elevated the maps' accuracy, leading to the average Kappa index of 0.83 (RGB) and 0.85 (MSP), and overall classification accuracy of 90 % for both approaches. Classification algorithm managed to distinguish aquatic vegetation with the almost perfect success rate of 0.84 for RGB and 0.95 Kappa index value for MSP approach. Producers and Users accuracy were 96.13% / 88.29% for RGB and 93.42% /97.18% for MSP workflow, respectfully. Classification accuracy of individual feature classes was generally higher for the MSP than for the RGB approach. In the MSP approach all but one aquatic vegetation feature class were 'almost perfectly' classified, while that was not the case for the RGB approach (Table 5). Finally, six aquatic vegetation maps were created based on the RGB, and five maps were created based on the MSP imagery. The total area and percentage of each feature class are presented in Table 6 and Figures 2-7.

5. DISCUSSION

5.1. Aquatic vegetation field survey

Results of the traditional monitoring approach, conducted on selected Danube transects, were in accordance with the data recorded during JDS4 along the Danube in Serbia realized the year before by the same researcher. The average time for the transect by boat was 30min during the JDS4, while the transect by foot required about an hour. A slightly shorter

Table 4. Training classification accuracy and accuracy of created digital maps.

		Training / 'per polygon' cl. accuracy				**Classification / 'per pixel' accuracy of digital maps**					
	Transect code	**KI CL**	**OA [%]**	**KI RC**	**OA [%]**	**KHI CL**	**OA [%]**	**KHI RC**	**OA [%]**	**KHI MERG**	**OA [%]**
RGB	Slatina_Bara	0.55	61	0.58	64	0.67	72	0.67	72	0.70	75
	Slatina_Dunav	0.65	75	0.67	77	0.67	78	0.75	85	0.75	85
	Dubovac_A	0.61	81	0.66	84	0.57	81	0.73	91	0.73	91
	Dubovac_B	0.55	80	0.71	87	0.89	97	0.87	96	0.87	96
	Labudovo okno	0.61	71	0.64	75	0.70	77	0.87	91	0.90	93
	Pančevo_A	0.86	93	0.91	96	0.95	98	0.98	99	0.98	99
	MEAN RGB	**0.64**	**77**	**0.70**	**80**	**0.74**	**84**	**0.81**	**89**	**0.82**	**90**
MSP	Slatina_Bara	0.58	63	0.63	68	0.54	61	0.67	72	0.71	77
	Slatina_Dunav	0.73	77	0.74	79	0.77	83	0.85	89	0.85	89
	Dubovc_A	0.70	81	0.81	89	0.84	93	0.90	97	0.90	97
	Dubovac_B	0.75	86	0.77	89	0.86	96	0.94	99	0.94	99
	Labudovo okno	0.68	74	0.73	77	0.73	79	0.80	85	0.86	90
	MEAN MSP	**0.69**	**76**	**0.74**	**80**	**0.75**	**83**	**0.83**	**88**	**0.85**	**90**

KI - Kappa index, OA - overall accuracy, KHI – Kappa hat index, CL – classification, RC – reclassification, MERG - digital maps with merged classes

Table 5. Classification accuracy of aquatic macrophytes feature classes.

			Submerged macrophytes		**Floating rooted macrophytes**			**Acropleustophytes**			**Helophytes**	
			Sbm veg	Alg / mud	Tra nat	Nym pel	Nuph /Nym	Sal nat	Sal/ Lem	Fil alg	Phra com	But umb
Average	RGB	PA [%]	88	90	92		98	30	87	43	90	
		UA [%]	83	70	87		71	50	100	41	57	
Average per Life form	RGB	**PA [%]**	**87**			**95**			**64**		**90**	
		UA [%]	**83**			**79**			**80**		**57**	
Average	MSP	PA [%]	74	66	97	99	95	79	96	69	94	
		UA [%]	77	75	99	99	83	100	95	97	91	
Average per Life form	MSP	**PA [%]**	**74**			**96**			**89**		**94**	
		UA [%]	**77**			**93**			**97**		**91**	

Table 6. Total area of each river transect with percentage covers [%] of each aquatic macrophyte class

		Area [ha]	Sbm veg	Alg / mud	Tra nat	Nym pel	Nuph /Nym	Sal nat	Sal/ Lem	Fil alg	Phra com	But umb
Slatina_Bara	RGB	9.9	15	13			15	3		<1	31	
Slatina_Dunav		24.0	10	7	13				3	2	1	1
Dubovac_A		16.6	20						1	<1	1	
Dubovac_B		10.2	15				1		1			
Labudovo okno		22.3	11	1	34	<1		<1		<1	5	
Pančevo_A		0.2	19									
Slatina_Bara	MSP	9.3	11	19			15	3		1	32	
Slatina_Dunav		20.8	9	12	14				4	2	<1	
Dubovac_A		12.6	13						1	<1	<1	
Dubovac_B		10.4	3				1		2			
Labudovo okno		16.7	11	1	36	<1		1		1	12	

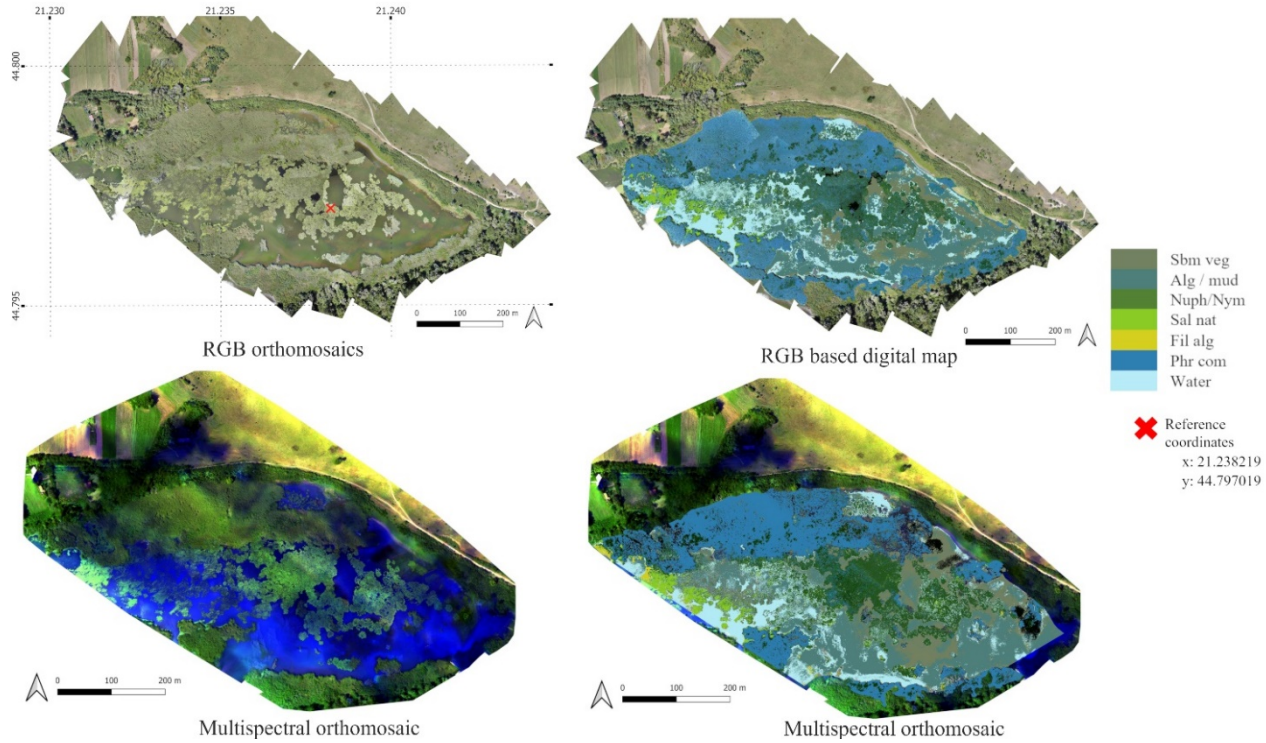

Figure 2. Ortohomosaics and digital maps of the Slatina (Bara) section

investigation time recorded during the JDS4 was probably due the lower abundance of macrophytes along the JDS river sections. eBee+ regular batteries can withstand 59 min of flight, while new smart batteries should go up to 90 min, so one battery should be able to sustain three 1 km transects in one flight, as is proposed by the JDS monitoring scheme for aquatic macrophytes, even in suboptimal flight conditions.

It should be mentioned that 300 m wide transects, which were used in this study, are too wide for most of the Danube River course, since aquatic vegetation develops mostly in the first 10 m from the riverbank. Extending the captured area towards the middle of the river in the absence of vegetation is not only redundant, but could negatively affect image processing, as uniform water areas are challenging for the creation of orthomosaics (Kislik et al., 2020).

Flight altitude in available studies (Brinkhoff et al., 2018; Flynn & Chapra, 2014; Taddia et al., 2020; Kislik et al., 2020; Ventura et al., 2018; Chabot et al., 2018) was notably lower than the flight height in this study. Resolution of the RGB orthomosaics was

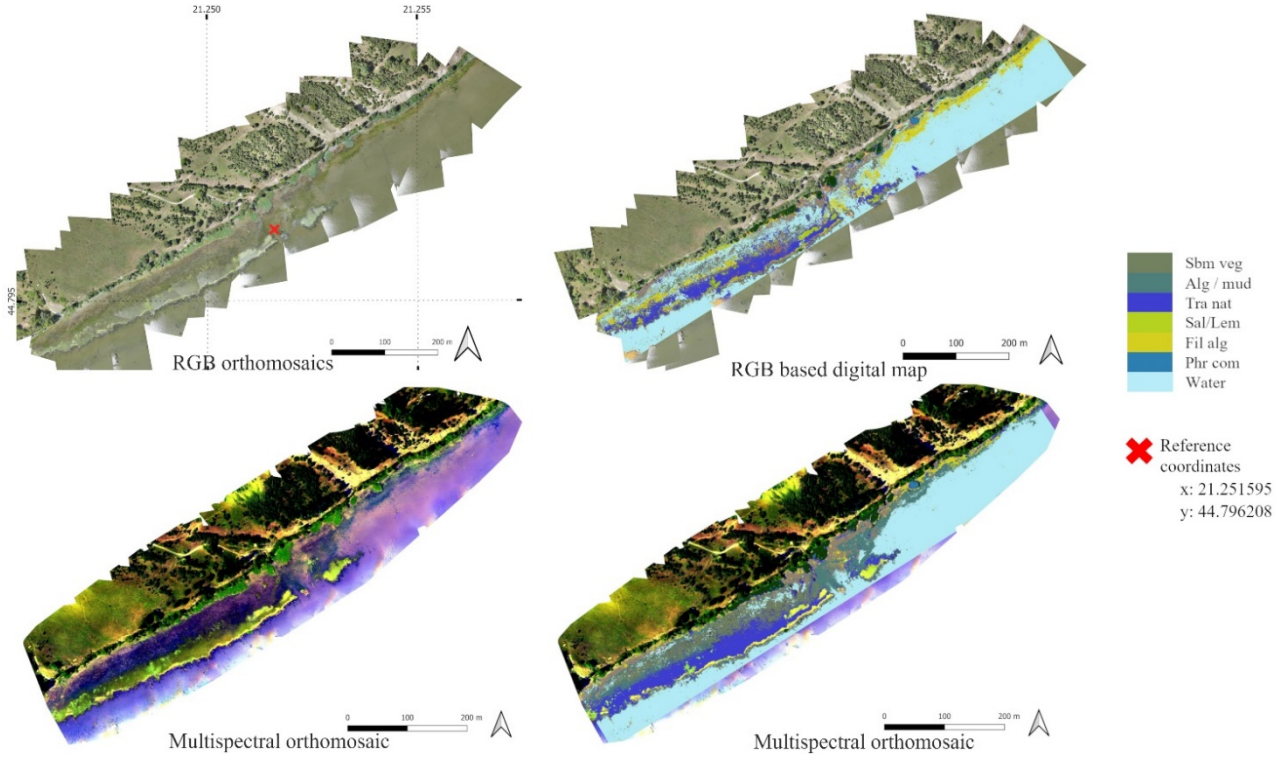

Figure 3. Ortohomosaics and digital maps of the Slatina (Dunav) river section

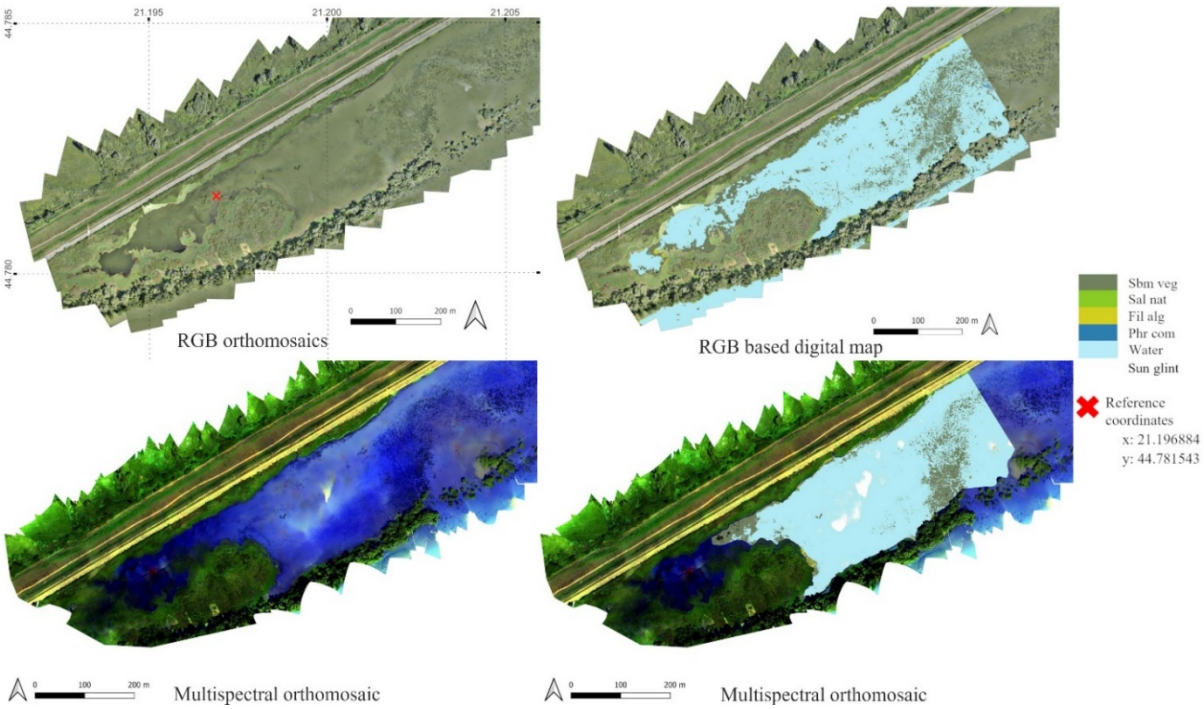

Figure 4. Ortohomosaics and digital maps of the Dubovac (A) river section

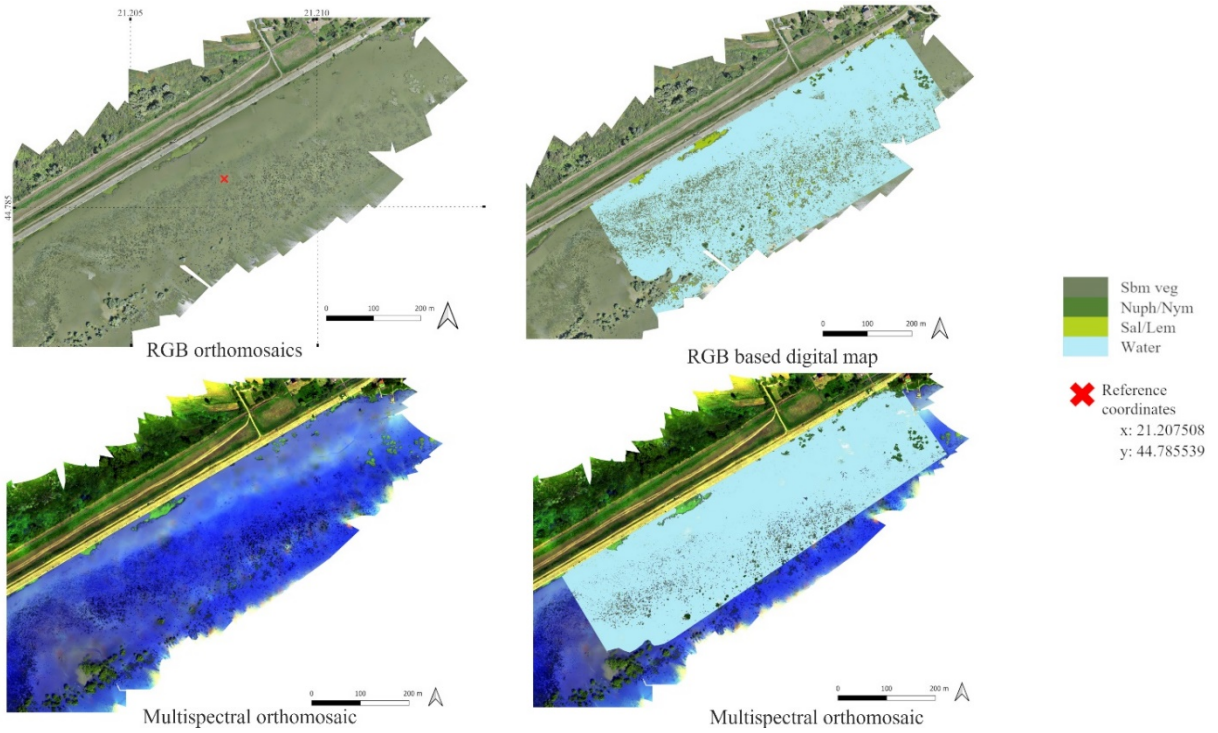

Figure 5. Ortohomosaics and digital maps of the Dubovac (B) river section

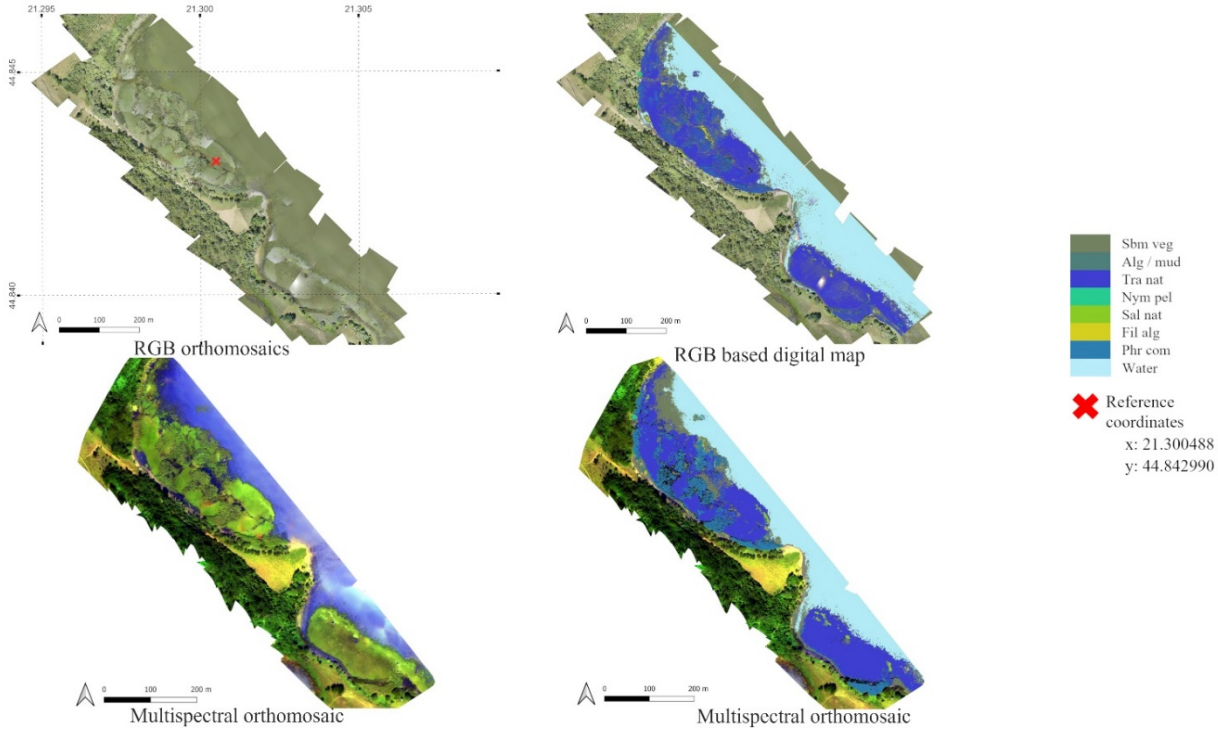

Figure 6. Ortohomosaics and digital maps of the Labudovo okno section

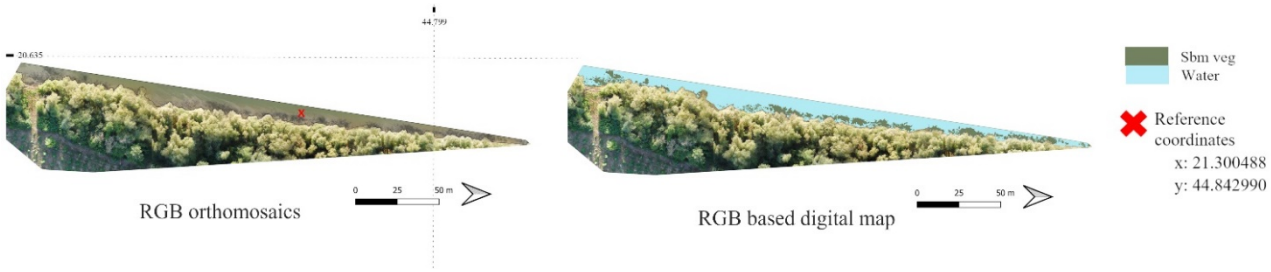

Figure 7. Ortohomosaics and digital maps of the Pančevo_A river section

completely satisfactory, while resolution of MSP ones should be better, in order to enable recognition of all desired image features without referring to the RGB data. Lowering the flight height to 120 m would result in adequate products resolution of 4 cm^2/pix.

5.2. UAV workflow

UAV image overlap was optimal for every survey site, resulting in successful creation of the orthomosaics. The RGB orthomosaic was only partially created at the Pančevo survey site, and the MSP images could not be processed successfully in either Pix4D or ArcGIS Pro software, which could be due to the presence of large uniform water areas. Taddia et al., (2020) also reported problems with orthomosaic generation, due to the large open water area. Kislik et al., (2020) even conducted single image analysis to bypass the problem. Such approach was not an option in this study because singular images would cover only a small percentage of the transect, while the aim was the creation of a vegetation map for each river transect.

Orthomosaic segmentation process was performed with low spectral range factors, which were selected based on the efficiency in distinguishing the patches of submerged vegetation. For the MSP approach the range factor needed to be decreased as the value used in the RGB workflow was unable to successfully delineate submerged vegetation. Similar issue was reported in Agioutanti, (2022), where the algorithm could not distinguish water from submerged algal patches. Low range factors caused sporadic oversegmentation, however these artefacts were further manageable by proper classification setup, unlike losing already frail information about submerged vegetation. Several authors also reported that a little oversegmentation is a better solution than undersegmentation, because it enables detail recognition and precise delineation of image features (De Luca et al., 2019; Díaz-Varela et al., 2018). In order to overcome this under-over-segmentation problem (Chabot et al., 2018; Ventura et al., 2018; Visser et al., 2018) propose multistage orthomosaic segmentation. Nevertheless, in this study the goal was the simplest and most straightforward mapping strategy so one-scale segmentation was applied.

Visual interpretation of the training and validation segments is recognized as a valid approach in aquatic vegetation UAV assisted mapping. Similar approaches were applied in Pande-Chhetri et al., (2017), Husson et al., (2017), Ventura et al., (2018) and Kislik et al., (2020). Despite the fact that field data was ancillary it was of substantial importance for the experts training and verification of UAV imagery interpretation, as noted in Chabot et al., (2016; 2018) as well.

Ideally, each of 22 macrophyte species would be represented with one image feature class within the classification process. In that way UAV vegetation monitoring would have the same resolution as the traditional methods. Due to technical constraints, combination of species-based and trait-based approaches resulted in 12 macrophyte feature classes, such as in many resembling studies (Husson et al., 2016; Chabot et al., 2016, 2018; Pande-Chhetri et al., 2017; Husson et al., 2017; Villoslada et al., 2020; Agioutanti, 2022). All submerged species were classified as 'submerged vegetation' feature class as in Chabot et al., (2016, 2018), Pande-Chhetri et al., (2017), Taddia et al., (2020) as it was not possible to determine the species due to the presence of mixed and complex vegetation stands, and poor spectral difference between them. Although there are studies focused on distinguishing and mapping specific submerged species (Brooks et al., 2019; Flynn & Chapra, 2014; Chabot et al., 2016, 2018; Ventura et al., 2018), information about submerged vegetation should always be carefully interpreted and may be considered scarce. Among the floating species, the yellow and white waterlily leaves were combined in one class, as in Husson et al., (2016; 2017). Lemnoid species could not be separated from *Salvinia natans* in the mixed stands, therefore the mixed group Sal/Lem was defined. Emergent species could be determined to the species level, but mostly because there were not any mixed vegetation stands or plethora of species present. *Trapa natans* class was divided in 'green' for regular individuals and 'red' for orange to red withering rosettes. In the same manner *Phragmites communis* classes were named 'green' and 'dry', but due to tall and vigorous emergent stems some fraction of the plants within the stands were 'shadowed'. When it comes to the Waterlilies, the regular 'green' leaf category was defined, but also there was the 'burnt' category for the leaves affected by the sun glint. For the MSP approach the 'burnt' class was omitted, as it was not necessary, most likely due the radiometric calibration of the images prior to analysis. Husson et al., (2016) used separate classes for dense and sparse macrophyte stands, while Pande-Chhetri et al., (2017) and Ventura et al., (2018) divided green and dry or dead plants. Within the MSP workflow additional image feature classes needed to be defined for the submerged vegetation. The category was divided into the 'deep' and 'subsurface' classes because of the different spectral and textural characteristics of the stands. Similarly, Chabot et al., (2018) divided floating and submerged plants of the same species into separate classes.

Optimization of the *Random Forest* classifier, by changing the algorithm parameters did not have a remarkable impact on the classification accuracy. In only two out of six investigated sites for RGB and none

for the MSP workflow, the change of parameters has led to the change of Kappa hat index category according to Landis and Koch, (1977). Similar patterns were also observed in (Chabot et al., 2018), while in the rest of available studies optimization phase was not conducted (Husson et al., 2016, 2017; van Iersel et al., 2018; Villoslada et al., 2020).

Aquatic vegetation was 'almost perfectly' distinguished from orthomosaics, with an average Producers accuracy (PA) of 95.8 % and Users accuracy (UA) of 88.1 % for RGB workflow, and 93.4 % and 97.2 % respectively for MSP workflow. These result were better or in line with the results of other studies which were mapping the aquatic vegetation *per se* (Husson et al., 2016; Brinkhoff et al., 2018; Kislik et al., 2020, Agioutanti, 2022). Usability of the final products - digital maps of aquatic macrophytes and life forms distribution was assessed using per-pixel accuracy. Classification accuracy of individual classes was generally higher in the MSP workflow. Within the MSP workflow all macrophyte classes were almost perfectly classified, except the Submerged vegetation which was highly 'substantially' accurate, while it was 'almost perfectly' classified within the RGB approach. Comparing with the other macrophytes, mapping of submerged vegetation using UAV technology appears to be quite challenging (Kislik et al., 2020; Agioutanti, 2022; Ventura et al., 2018), especially within the MSP workflow. Chabot et al., (2018) used the 'rule-based feature extraction tools' to delineate submerged and above-water image features. In the same manner, Visser et al., (2018) used rule set OBIA and reported rather variable results, but nevertheless recognized the potential of OBIA in high-resolution image classification. Floating and free-floating classes predominantly had excellent classification accuracy in this study. Similar values were reported by Chabot et al., (2018) mapping invasive species in aquatic habitats using MSP imagery, while available RGB studies obtained slightly poorer results (Husson et al., 2016; Husson et al., 2017; Pande-Chhetri et al., 2017). *Phragmites communis* class obtained only moderate classification accuracy within the RGB workflow, while in the MSP workflow it was almost perfectly classified. This discrepancy could possibly be caused by coarser GSD of the photogrammetry products (~8 cm/pix) and therefore less details within the stands, but also due to the calculation of the additional spectral indices which ware enabled by NIR and RedEdge band Emergent vegetation in other studies has shown similar or higher accuracy (Husson et al., 2016, 2017; Pande-Chhetri et al., 2017; van Iersel et al., 2018). All of the named studies had poorer GSD (>5 cm/pix). *Nymphoides peltata* and *Butomus umbelatus* classes accuracy were not assessed within the RGB workflow, as both groups were present in only one river transect with no more than 1 % of the area, therefore none of the randomly selected validation polygons included segments of these classes.

6. CONCLUSION

Joint Danube Survey macrophyte assessment guidance assumes the evaluation of aquatic vegetation on six survey units at each sampling location, three 1km transects on the left and three on the right riverbank according to the European standard CEN EN-14184:2014. In that manner only a relative measure of the species' presence and plant life forms at each river kilometer is recorded. Introduction of the UAV approach would enable the assessment of the total area covered with aquatic macrophytes and result in the absolute cover values opposing to the relevant ones using the traditional methods. On the other hand, with a realistic insight into the terrain and habitat types, it would be possible to perform a more precise intercalibration of the sampling methodology as well as the assessment of the condition of distant and typologically different sections of large hydrosystems such as the Danube. This methodology could also be used to monitor aquatic vegetation of moors, flood zones and wet areas along rivers, the research of which represents a methodological challenge, and is very often absent, despite being considered the centres of biodiversity of river ecosystems.

Recommendations:

- Fixed-winged UAV drones carrying multispectral or combined multispectral/RGB cameras.
- Resolution of the photogrammetry products~3 cm/pix is adequate for the mapping of aquatic vegetation. Determining the photogrammetry products' resolution should be cautiously performed. A too high imagery resolution could lead to noise saturated orthomosaics and to large and computationally challenging orthomosaic.
- Before the flight, each river stretch should be inspected using low-cost small copter-type drone to determine transect dimensions.
- Flights can be planned just before each take off as it takes only several minutes, but potential take-off and landing location should be chosen prior to field work.
- Longitudinal overlap of 80 % and lateral of 60 % showed satisfactory results. In the situations when large uniform areas need to be assessed, an increase of the image overlap could enable successful orthomosaic creation. Photos containing only open water, or homogenous riparian forest are challenging to process and therefore should not be captured if possible.
- For the purposes of the ground truthing of the aquatic

vegetation, modification of the sampling strategy could be performed. Standard transect approach supplemented with modified per plot approach could be implemented. Rather than collecting a full vegetation plot data at every stop, only coordinates of the dominant target species could be recorded. In that way macrophyte species and groups spatial and temporal patterns could be collected and studied.

- This survey approach enables reliable and unbiased field data collection by researchers, technicians, and practitioners requiring only basic knowledge about species taxonomy and GIS/UAV technology.
- MSP images should be preprocessed, adjusted, and geotagged using suitable software. Also, whenever possible, images should be radiometrically calibrated.
- The combination of the OBIA classification and Random Forest algorithm, showed to be suitable and was also easily manageable approach.
- During the segmentation process, the appropriate spectral difference factor should be chosen. In order to distinguish macrophyte classes, quite small spectral differences should be considered as threshold values, as aquatic macrophytes tend to have similar spectral signatures.
- Training and validation datasets should be created based on expert's knowledge rather than on excessive traditional field work campaigns.
- Flight missions should be performed before the traditional assessment methods. In this way the flight itself could be used as input about the aquatic vegetation distribution and variation along the transect.

Acknowledgments:

This study was supported by the Rufford grant No 28388-1; by the project of Provincial Secretariat for Higher Education and Scientific Research, Autonomous Province of Vojvodina, Republic of Serbia, no 142-451-2095/2022-01; by the Ministry of Science, Technological Development, and Innovation of the Republic of Serbia (Grant No. 451-03-47/2023-01/200125).

REFERENCE

Agioutanti R., 2022. *Classifying and Mapping Aquatic Vegetation in Heterogeneous Stream Ecosystems Using Visible and Multispectral UAV Imagery.* University of Kentucky. https://doi.org/10.13023/etd.2022.034

Barbosa, B. D. S., Ferraz, G. A. S., Gonçalves, L. M., Marin, D. B., Maciel, D. T., Ferraz, P. F. P., & Rossi, G., 2019. *RGB vegetation indices applied to grass monitoring: A qualitative analysis.* Agronomy Research, 17, 2, 349–357. https://doi.org/10.15159/AR.19.119

Bendig, J., Kang, Y., Helge, A., Andreas, B., Simon, B., Janis, B., Martin, L.G., & Georg, B., 2015. *Combining UAV-based plant height from crop surface models, visible, and near infrared vegetation indices for biomass monitoring in barley.* International Journal of Applied Earth Observation and Geoinformation, 39, 79-87. https://doi.org/10.1016/j.jag.2015.02.012.

Birk, S., Bonne, W., Borja, A., Brucet, S., Courrat, A., Poikane, S., Solimini, A., Van De Bund, W., Zampoukas, N., & Hering, D., 2012. *Three hundred ways to assess Europe's surface waters: An almost complete overview of biological methods to implement the Water Framework Directive.* Ecological Indicators, 18, 31-41. https://doi.org/10.1016/j.ecolind.2011.10.009

Birk, S., Strackbein, J. & Hering, D., 2010**.** WISER methods database. Version: March 2011. Available at http://www.wiser.eu/results/method-database/. [Accessed, 17.03.2020.]

Bolch, E. A., Hestir, E. L., & Khanna, S., 2021. *Performance and feasibility of drone-mounted imaging spectroscopy for invasive aquatic vegetation detection.* Remote Sensing, 13, 4, 1–20. https://doi.org/1 0.3390/rs13040582

Brinkhoff, J., Hornbuckle, J., & Barton, J. L., 2018. *Assessment of aquatic weed in irrigation channels using UAV and satellite imagery.* Water, 10, 11, 1–20. https://doi.org/10.3390/w10111497

Brooks, C. N., Grimm, A. G., Marcarelli, A. M., & Dobson, R. J., 2019. *Multiscale collection and analysis of submerged aquatic vegetation spectral profiles for Eurasian watermilfoil detection.* Journal of Applied Remote Sensing, 13, 03, 1. https://doi.org/10.1117/1.jrs.13.037501

Chabot, D., Dillon, C., Shemrock, A., Weissflog, N., & Sager, E. P. S., 2018. *An object-based image analysis workflow for monitoring shallow-water aquatic vegetation in multispectral drone imagery.* ISPRS International Journal of Geo-Information, 7, 8. https://doi.org/10.3390/ijgi7080294

Chabot, D., Dillon, C., Ahmed, O., & Shemrock, A., 2016. *Object-based analysis of uas imagery to map emergent and submerged invasive aquatic vegetation: A case study.* Journal of Unmanned Vehicle Systems, 5, 1, 27–33. https://doi.org/10.1139/juvs-2016-0009

De Luca, G., Silva, J. M. N., Cerasoli, S., Araújo, J., Campos, J., Di Fazio, S., & Modica, G., 2019. *Object-based land cover classification of cork oak woodlands using UAV imagery and Orfeo Toolbox.* Remote Sensing, 11, 10. https://doi.org/10.3390/rs11101238

De Marinis, P., De Petris, S., Sarvia, F., Manfron, G., Momo, E. J., Orusa, T., Corvino, G., Sali, G., & Borgogno, E. M., 2021. *Supporting pro-poor reforms of agricultural systems in eastern DRC (Africa) with remotely sensed data: A possible contribution of spatial entropy to interpret land management practices.* Land, 10, 12, 1368. https://doi.org/10.3390/land10121368

Díaz-Varela, R. A., Calvo Iglesias, S., Cillero Castro, C., & Díaz Varela, E. R., 2018. *Sub-metric analisis of*

vegetation structure in bog-heathland mosaics using very high resolution rpas imagery. Ecological Indicators, 89, 861–873. https://doi.org/10.1016/j.ecolind.2017.11.068

Flynn, K. F., & Chapra, S. C., 2014. *Remote sensing of submerged aquatic vegetation in a shallow non-turbid river using an unmanned aerial vehicle.* Remote Sensing, 6, 12, 12815–12836. https://doi.org/10.3390/rs61212815

Gitelson, A., Kaufman, Y.J. & Merzlyak, M.N., 1996. *Use of a Green Channel in Remote Sensing of Global Vegetation from EOS-MODIS*. Remote Sensing of Environment, 58, 289–298. https://doi.org/10.1016/S0034-4257(96)00072-7

Gitelson, A., & Merzlyak, M.N., 1994. *Quantitative estimation of chlorophyll-a using reflectance spectra: Experiments with autumn chestnut and maple leaves.* Journal of Photochemistry and Photobiology, B 22, 247–252. https://doi.org/10.1016/1011-1344(93)06963-4

Huang, X., Zhang L., & Li P., 2007. *Classification and Extraction of Spatial Features in Urban Using High-Resolution Multispectral Imagery*. IEEE Geoscience and Remote Sensing Letters, 4, 2, 260-264. DOI: 10.1109/LGRS.2006.890540

Husson, E., Ecke, F., & Reese, H., 2016. *Comparison of manual mapping and automated object-based image analysis of non-submerged aquatic vegetation from very-high-resolution UAS images.* Remote Sensing, 8, 9, 1–18. https://doi.org/10.3390/rs8090724

Husson, E., Hagner, O., & Ecke, F., 2014. *Unmanned aircraft systems help to map aquatic vegetation.* Applied Vegetation Science, 17, 3, 567–577. https://doi.org/10.1111/avsc.12072

Husson, E., Reese, H., & Ecke, F., 2017. *Combining spectral data and a DSM from UAS-images for improved classification of non-submerged aquatic vegetation*. Remote Sensing, 9, 3, 247. https://doi.org/10.3390/rs9030247

Jaskuła, J., & Sojka, M., 2019. *Application Of Remote Sensing and Gis To Water Transparency Estimation In Reservoirs.* Carpathian Journal of Earth and Environmental Sciences, 14, 2, 353–366. DOI:10.26471/cjees/2019/014/086

JDS4. 2021. *Joint Danube Survey 4. Scientific Report: A Shared Analysis of the Danube River*. *Report: JDS4*

Jiménez-Jiménez, S. I., Ojeda-Bustamante, W., Ontiveros-Capurata, R. E., & Marcial-Pablo, M. de J., 2020. *Rapid urban flood damage assessment using high resolution remote sensing data and an object-based approach.* Geomatics, Natural Hazards and Risk, 11, 1, 906–927. https://doi.org/10.1080/19475705.2020.1760360

Kaplan, G., Milevski, I., & Valjarević, A., 2022. *National Land Cover Mapping Using Various Remote Sensing Datasets In Gee.* Carpathian Journal of Earth and Environmental Sciences, 17, 2, 297–306. DOI: 10.26471/cjees/2022/017/223

Kislik, C., Genzoli, L., Lyons, A., & Kelly, M., 2020. *Application of UAV imagery to detect and quantify submerged filamentous algae and rooted macrophytes in a non-wadeable river*. Remote Sensing, 12, 20, 1–24. https://doi.org/10.3390/rs12203332

Kohler, A. & Janauer G.A., 1995. *Zur Methodik der Untersuchung von aquatischen Makrophyten in Fließgewässern*; In: Steinderg C, Bernhardt H. und Klapper H., Handbuch Angewandte Limnologie, Kap. VIII - 1.1.3. Ecomed-Verlag, Landsberg/Lech, 1-22.

Kohler, A., 1978. *Methoden der Kartierung von Flora und Vegetation von Süwasserbiotopen*. Landschaft+Stadt 10, 73–85.

Kupidura, P., 2019. *The comparison of different methods of texture analysis for their efficacy for land use classification in satellite imagery*. Remote Sensing, 11, 10, 1233. https://doi.org/10.3390/rs11101233

Landis, J.R., & Koch, G.G., 1997. *The measurement of observer agreement for categori-cal data*. Biometrics, 33, 159–174. https://doi.org/10.2307/2529310

Louhaichi, M., Borman, M.M. & Johnson, D.E., 2001. *Spatially Located Platform and Aerial Photography for Documentation of Grazing Impacts on Wheat*. Geocarto International, 16, 1, 65–70. https://doi.org/10.1080/10106040108542184

Ma, L., Li, M., Ma, X., Cheng, L., Du, P., & Liu, Y., 2017. *A review of supervised object-based land-cover image classification.* In ISPRS Journal of Photogrammetry and Remote Sensing, 130, 277-293. https://doi.org/10.1016/j.isprsjprs.2017.06.001

Manfreda, S., McCabe, M. F., Miller, P. E., Lucas, R., Pajuelo Madrigal, V., Mallinis, G., … Toth, B., 2018. *On the Use of Unmanned Aerial Systems for Environmental Monitoring*. Remote sensing, 10, 4, 641 https://doi.org/10.3390/rs10040641

Marcaccio, J. V., Markle, C. E., & Chow-Fraser, P., 2015. *Unmanned aerial vehicles produce high-resolution, seasonally-relevant imagery for classifying wetland vegetation.* ISPRS Archives, 174: 609-615. https://doi.org/10.5194/isprsarchives-XL-1-W4-249

McFeeters, S. K., 1996. *The use of the Normalized Difference Water Index (NDWI) in the delineation of open water features.* International Journal of Remote Sensing, 17, 7, 1425–1432. https://doi.org/10.1080/01431169608948714

Michez, A., Piégay, H., Jonathan, L., Claessens, H., & Lejeune, P., 2016. *Mapping of riparian invasive species with supervised classification of Unmanned Aerial System (UAS) imagery.* International Journal of Applied Earth Observation and Geoinformation. https://doi.org/10.1016/j.jag.2015.06.014

MIDCC. https://www.midcc.at/ [Acessed, june 2022]

Pande-Chhetri, R., Abd-Elrahman, A., Liu, T., Morton, J., & Wilhelm, V. L., 2017. *Object-based classification of wetland vegetation using very high-resolution unmanned air system imagery.* European Journal of Remote Sensing, 50, 1, 564–576. https://doi.org/10.1080/22797254.2017.1373602

Pearson, R.L.; Miller, L.D., 1972. *Remote mapping of standing crop biomass for estimation of the productivity of the shortgrass prairie.* In Proceedings of the Eighth International Symposium on Remote

Sensing of Environment, University of Michigan, Ann Arbor, MI, USA, 2–6 October 1972, 1357–1381.

Rouse, J.W., Haas, R.H., Schell, J.A., & Deering, D.W., 1973. *Monitoring vegetation systems in the Great Plains with ERTS.* In Proceedings of the 3th Earth Resources Technology Satellite-1 Symposium, Goddard Space Flight Center, NASA, Washington, DC, USA, 10–14 December 1973, 309–317.

Sibaruddin, H. I., Shafri, H. Z. M., Pradhan, B., & Haron, N. A., 2018. *Comparison of pixel-based and object-based image classification techniques in extracting information from UAV imagery data.* IOP Conference Series: Earth and Environmental Science, 169, 1. https://doi.org/10.1088/1755-1315/169/1/012098

Sojka, M., Jaskuła, J., Wrózyński, R., & Waligórski, B., 2019. *Application of sentinel-2 Satellite imagery to assessment of spatio-temporal changes in the reservoir overgrowth process - A case study: Przebędowo, West Poland.* Carpathian Journal of Earth and Environmental Sciences, 14, 1, 39–50. https://doi.org/10.26471/cjees/2019/014/056

Song, B., & Park, K., 2020. *Detection of aquatic plants using multispectral UAV imagery and vegetation index.* Remote Sensing, 12, 3, 1–16. https://doi.org/10.3390/rs12030387

Stehman, S. V., & Wickham, J. D., 2011. *Pixels, blocks of pixels, and polygons: Choosing a spatial unit for thematic accuracy assessment.* Remote Sensing of Environment, 115, 12, 3044–3055. https://doi.org/10.1016/j.rse.2011.06.007

Stocks, J. R., Rodgers, M. P., Pera, J. B., & Gilligan, D. M., 2019. *Monitoring aquatic plants: An evaluation of hydroacoustic, on-site digitising and airborne remote sensing techniques.* Knowledge & Management of Aquatic Ecosystems, 420, 27. https://doi.org/10.1051/kmae/2019016

Taddia, Y., Russo, P., Lovo, S., & Pellegrinelli, A., 2020. *Multispectral UAV monitoring of submerged seaweed in shallow water.* Applied Geomatics, 12, 19–34. https://doi.org/10.1007/s12518-019-00270-x

Tmušić, G., Manfreda, S., Aasen, H., James, M. R., Gonçalves, G., Ben-Dor, E., Brook, A., Polinova, M., Arranz, J. J., Mészáros, J., Zhuang, R., Johansen, K., Malbeteau, Y., de Lima, I. P., Davids, C., Herban, S., & McCabe, M. F., 2020. *Current Practices in UAS-based Environmental Monitoring.* Remote Sensing, 12, 6, 1001. https://doi.org/10.3390/rs12061001

Tucker, C.J., 1979. *Red and photographic infrared linear combinations for monitoring vegetation.* Remote Sensing of Environment, 8, 127–150. https://doi.org/10.1016/0034-4257(79)90013-0

van Iersel, W., Straatsma, M., Middelkoop, H., & Addink, E., 2018. *Multitemporal classification of river floodplain vegetation using time series of UAV images.* Remote Sensing, 10, 7, 1144. https://doi.org/10.3390/rs10071144

Ventura, D., Bonifazi, A., Gravina, M. F., Belluscio, A., & Ardizzone, G., 2018. *Mapping and classification of ecologically sensitive marine habitats using unmanned aerial vehicle (UAV) imagery and Object-Based Image Analysis (OBIA).* Remote Sensing, 10, 9, 1–23. https://doi.org/10.3390/rs10091331

Villa, P., Bresciani, M., Braga, F., & Bolpagni, R., 2014. *Comparative assessment of broadband vegetation indices over aquatic vegetation.* IEEE Journal of Selected Topics in Applied Earth Observations and Remote Sensing, 7, 7, 3117–3127. https://doi.org/10.1109/JSTARS.2014.2315718

Villoslada, M., Bergamo, T. F., Ward, R. D., Burnside, N. G., Joyce, C. B., Bunce, R. G. H., & Sepp, K., 2020. *Fine scale plant community assessment in coastal meadows using UAV based multispectral data.* Ecological Indicators, 111, 105979. https://doi.org/10.1016/j.ecolind.2019.105979

Visser, F., Wallis, C., & Sinnott, A. M., 2013. *Optical remote sensing of submerged aquatic vegetation: Opportunities for shallow clearwater streams.* Limnologica, 43, 5, 388–398. https://doi.org/10.1016/j.limno.2013.05.005

Visser, F., Buis, K., Verschoren, V., & Schoelynck, J., 2018. *Mapping of submerged aquatic vegetation in rivers from very high-resolution image data, using object-based image analysis combined with expert knowledge.* Hydrobiologia, 812, 1, 157–175. https://doi.org/10.1007/s10750-016-2928-y

Visser, F., Buis, K., Verschoren, V., & Meire, P., 2015. *Depth estimation of submerged aquatic vegetation in clear water streams using low-altitude optical remote sensing.* Sensors, 15, 10, 25287–25312. https://doi.org/10.3390/s151025287

Woebbecke, D.M., Meyer, G.E., Von Bargen, K. & Mortensen, D.A., 1995. *Color indices for weed identification under various soil, residue, and lighting conditions.* Transactions of the ASAE, 38,1, 259–269.

Yang, Z., Willis, P., & Mueller, R., 2008. *Impact of Band-Ratio Enhanced AWIFS Image on Crop Classification Accuracy.* United States Department of Agriculture. National Agricultural Statistics Service. Research and Development Division. 3251 Old Lee Highway, Room 305. Fairfax, VA 22030

Ye, S., Pontius, R. G., & Rakshit, R., 2018. *A review of accuracy assessment for object-based image analysis: From per-pixel to per-polygon approaches.* ISPRS Journal of Photogrammetry and Remote Sensing, 141, 137–147. https://doi.org/10.1016/j.isprsjprs.2018.04.002

Received at: 18. 04. 2023
Revised at: 07. 05. 2023
Accepted for publication at: 17. 06. 2023
Published online at: 27. 06. 2023